Journal of
Applied Remote Sensing

Lidar investigations on the optical and dynamical properties of cirrus clouds in the upper troposphere and lower stratosphere regions at a tropical station, Gadanki, India (13.5°N, 79.2°E)

Vasudevannair Krishnakumar
Malladi Satyanarayana
Soman R. Radhakrishnan
Reji K. Dhaman
Glory Selvan Jayeshlal
Gopinathan Nair S. Motty
Vellara P. Mahadevan Pillai
Karnam Raghunath
Madineni Venkat Ratnam
Duggirala Ramakrishna Rao
Pindlodi Sudhakar

SPIE

Lidar investigations on the optical and dynamical properties of cirrus clouds in the upper troposphere and lower stratosphere regions at a tropical station, Gadanki, India (13.5°N, 79.2°E)

Vasudevannair Krishnakumar,[a,b] Malladi Satyanarayana,[a,*] Soman R. Radhakrishnan,[c] Reji K. Dhaman,[a] Glory Selvan Jayeshlal,[a] Gopinathan Nair S. Motty,[a] Vellara P. Mahadevan Pillai,[a] Karnam Raghunath,[d] Madineni Venkat Ratnam,[d] Duggirala Ramakrishna Rao,[e] and Pindlodi Sudhakar[e]

[a]University of Kerala, Department of Optoelectronics, Kariavattom, Trivandrum 695581, Kerala, India

[b]Mohandas College of Engineering and Technology, Anad, Thiruvananthapuram 695544, India

[c]CSIR-National Physical Laboratory, Radio and Atmospheric Sciences Division, Dr. K. S. Krishnan Road, New Delhi 110012, India

[d]National Atmospheric Research Laboratory, Gadanki, Tirupati 517502, India

[e]Geetanjali College of Engineering and Technology, Cheeryal, Keesara, Hyderabad 501301, Andhra Pradesh, India

Abstract. High altitude cirrus clouds are composed mainly of ice crystals with a variety of sizes and shapes. They have a large influence on Earth's energy balance and global climate. Recent studies indicate that the formation, dissipation, life time, optical, and micro-physical properties are influenced by the dynamical conditions of the surrounding atmosphere like background aerosol, turbulence, etc. In this work, an attempt has been made to quantify some of these characteristics by using lidar and mesosphere–stratosphere–troposphere (MST) radar. Mie lidar and 53 MHz MST radar measurements made over 41 nights during the period 2009 to 2010 from the tropical station, Gadanki, India (13.5°N, 79.2°E). The optical and microphysical properties along with the structure and dynamics of the cirrus are presented as observed under different atmospheric conditions. The study reveals the manifestation of different forms of cirrus with a preferred altitude of formation in the 13 to 14 km altitude. There are considerable differences in the properties obtained among 2009 and 2010 showing significant anomalous behavior in 2010. The clouds observed during 2010 show relatively high asymmetry and large multiple scattering effects. The anomalies found during 2010 may be attributed to the turbulence noticed in the surrounding atmosphere. The results show a clear correlation between the crystal morphology in the clouds and the dynamical conditions of the prevailing atmosphere during the observational period. [DOI: 10.1117/1.JRS.8.083659]

Keywords: lidar; cirrus optical properties; cirrus symmetry; lasers remote sensing.

Paper 13395 received Oct. 18, 2013; revised manuscript received Jan. 23, 2014; accepted for publication Feb. 18, 2014; published online Mar. 26, 2014.

1 Introduction

Clouds play a crucial role in maintaining the hydrological and radiative balances that are necessary for the existence of life on Earth. Among these, cirrus clouds are major regulators of Earth's radiation budget and they act like greenhouse gasses. Typically, they reflect short-wave radiation of solar spectrum back to space and also the long-wave radiation emitted

*Address all correspondence to: Malladi Satyanarayana, E-mail: drsatyanarayana.malladi@gmail.com

0091-3286/2014/$25.00

by Earth back toward the ground. The composition and structure of cirrus clouds play an important role in the radiative forcing offered by them. These upper tropospheric ice phase clouds (cirrus clouds) are characterized by their extensive lateral and vertical coverage.[1] Cirrus clouds can impose a large-scale radiative effect on the Earth's climate system, as 1/5th of the global tropics are regularly covered by extensive cirrus systems.[2]

It is known that the formation, life-span, decay, and the optical properties of the clouds are influenced by the anthropogenic and nonanthropogenic contents and dynamics of the surrounding atmosphere. The role of the prevailing atmospheric conditions on the macroscopic properties of the clouds, their extent, precipitation efficiency, radiative properties, and life time is of great interest in the cloud-climate study. Moreover, the short time dynamical behavior of the atmosphere alters the optical properties and time history of the clouds considerably. Thus the radiative properties of the clouds get modified because of the dynamical conditions of the atmosphere. However, the experimental data on some of these aspects are sparse. For example, the effect of the turbulence on the cloud properties is not well understood, at least in the tropics. Turbulence is important because it mixes and churns the atmosphere and causes water vapor, smoke, and other substances, as well as energy, to become distributed both vertically and horizontally. As such it is desirable to measure the turbulence characteristics of the surrounding atmosphere simultaneously along with the optical properties of the cirrus clouds with a view to understanding the basic mechanisms of the formation and dissipation of the clouds. In this study, we present the results on these aspects making use of the lidar and radar measurements at a tropical station Gadanki, India (13.5°N, 79.2°E). Lidar measurements are used to derive the optical properties of the cirrus. The atmospheric turbulence is obtained by using the refractive index profile derived from a static Hufnagel model.[3,4] The 53 MHz MST radar operational at the site is used to derive the vertical wind velocity component to give the turbulence in the upper troposphere and lower stratosphere (UTLS) regions.

Periodic variation of cirrus cloud geometry, depolarization ratio, lidar ratio (LR), and cloud asymmetry observed from the station is been thoroughly investigated for the period 2009 to 2010 in Secs. 2–4.2. It is hypothesized from the findings of the work that the cloud geometry and its microphysical properties vary significantly with respect to the dynamical variability like turbulence, etc. The effect of turbulence on cloud symmetry and LR is discussed in Secs. 4.3 and 5. Here, turbulence is assimilated by using Hufnagel-Valley model and MST radar velocity component profiles. The Hufnagel-Valley model is discussed in line with MST radar wind velocity component derived from the radar signal in Sec. 4.2. The main objective of this work is to establish the relationship between the dynamical variability turbulence and cloud physical properties like cloud symmetry and LR.

2 Experimental Methods

2.1 *Lidar Description*

The experiments are carried out using the elastic back scatter lidar system operational on a regular basis at NARL, Gadanki.[5] The lidar transmitter employs a Nd:YAG laser which emits the laser radiation (frequency doubled) at a wavelength of 532 nm and with an energy of 550 mJ/pulse (pulse-width—7 ns and repetition rate—20 Hz). The laser beam is expanded using a 10× beam expander, which makes the beam divergence <0.1 mrad. The receiver telescope is a 350-mm diameter Schmidt–Cassegrain-type telescope with an FOV of 1 mrad. This is used to study the vertical structure of atmospheric aerosols by receiving the Mie scattered signal.

A narrow-band interference filter with center wavelength of 532 nm is used to minimize the noise from the sky background radiation. The receiver has the depolarization measurement capability. A polarized beam splitter splits the beam into parallel and perpendicular components and are recorded separately using two independent and identical photomultiplier tube (PMT) channels, which are referred to as parallel (P) and cross (S) channels, respectively. PMT saturation is avoided by introducing the variable attenuators in the channels. The optical power received by these two PMTs is recorded separately by two photon counters. Recording of data is achieved with a four-channel-PC based data acquisition system, out of which two

channels each are reserved for data acquisition from each telescope. In this work, the data up to 20 km from the Mie lidar were used for measuring the vertical profiles of depolarization ratios and extinction coefficients from the background aerosol and clouds corresponding to the period from January 2009 to December 2010. Simultaneous data on atmospheric pressure, humidity, and temperature are taken from radiosonde experiments conducted at the station during the period. During the period January 2009 to December 2010, lidar observations are made on 41 nights.

2.2 *Mesosphere-Stratosphere-Troposphere Radar*

The Indian MST radar is monostatic coherent pulse Doppler radar operating at 53 MHz with a peak-power aperture product of 3×10^{10} Wm^2 and is located at Gadanki, India.[6] The antenna system occupying an area of 130 m $\times$ 130 m is a phased array of 32×32 three-element Yagi antennas consisting of two orthogonal sets, one for each polarization (magnetic E–W and N–S). It generates a radiation pattern with the main lobe of 3 deg width (between 3 dB points), gain of 36 dB, and first side lobe level of -20 dB. The main beam can be positioned at any look angle within ± 20 deg off zenith in the two major planes (E–W and N–S). The number of fast Fourier transform (FFT) points is up to 512 and coherent integrations are also up to 512 (selectable in binary steps). The pulse widths can be decoded from 1 to 32 μs (in binary steps) and can be coded from 16 to 32 μs with 1 μs band length. The pulse width employed here is 16 μs. Radar specifications and other important parameters used for the present study are given in Table 1.

3 Method of Analysis

3.1 *Lidar Data Analysis*

Location of lidar site is Gadanki (13.5°N, 79.2°E; 375-m mean sea level) situated close to Tirupati, in the southern part of India. The lidar signal was analyzed on the basis of lidar equation for two distinct classes of scatters[7] is

$$P(z) = ECZ^{-2}[\beta_1(Z) + \beta_2(Z)]T_1^2(Z)T_2^2(Z),$$

where $P(Z)$ is the return signal that is proportional to the received power from a scattering volume at slant range Z, E is an output energy monitor pulse which is proportional to the transmitted energy, C is the calibration constant of the instrument which includes losses in the transmitting and receiving optics and the effective receiver aperture, $\beta_1(Z)$ and $\beta_2(Z)$ are the backscattering cross sections of the aerosols and molecules at slant range Z, $T_1(Z)$ is the aerosol transmittance

Table 1 Radar specifications and other important parameters of the Indian MST radar facility.

Parameter	Specification
Power aperture product (peak)	3×10^{10} Wm^2
Beam width	3 deg
Pulse width	16 μs
Inter pulse period	1000 μs
No. of FFT point	128
No. of coherent integration	64
No. of coherent integration	2
Range resolution	2.4 km
Number of beams	Five (E, W Zenith Y, N and S)

and $T_2(Z)$ is the molecular atmosphere transmittance. The properties like the molecular scattering cross section and the extinction cross section for the atmospheric molecules are derived from the rocket sounding experiments conducted by Sasi et al.[8] Further simplifying assumption is that the aerosol extinction-to-backscattering is taken as a constant of about 20 for the inland station. The molecular extinction-to-backscattering ratio is taken as $8(\pi/3)$.[7] The lidar data can, therefore, be analyzed in successive steps discussed as in Fernalds[7] method to derive the range resolved extinction and backscattering. Aerosol optical depth (τ) is calculated by integrating the extinction coefficient from bottom to top of the observation column

$$\tau = \int_{r_1}^{r_2} \alpha_{\mathrm{a}}(r)\mathrm{d}r,$$

where α_a is the aerosol extinction coefficient. Cloud optical depth (τ_c) is calculated by integrating the extinction coefficient from cloud base to its top as

$$\tau_{\mathrm{c}} = \int_{r_1}^{r_2} \alpha(r)\mathrm{d}r,$$

where $\alpha(r)$ is the cloud extinction coefficient. Cirrus clouds are generally classified on the basis of optical depth values. We adopted the classification made by Sassen and Cho[9] for characterizing the upper tropospheric clouds (at 690 nm), which is an accepted model for cirrus cloud classification. According to this classification, cirrus clouds having $\tau_{\mathrm{c}} \leq 0.03$ are classified as subvisible cirrus. Clouds having optical depth in the range $0.03 < \tau_c \leq 0.3$ are classified as thin cirrus (TC) and clouds with $\tau_{\mathrm{c}} > 0.3$ are dense cirrus (DC). The linear depolarization ratio (LDR), $\delta(r)$ of the backscattered radiation, which is defined as the ratio of total backscattering coefficient of the cross polarized signal to that of the copolarized signal, can be written as[10]

$$\delta(r) = \delta_{\mathrm{m}} \frac{R_{\mathrm{s}}(r)}{R_{\mathrm{p}}(r)}$$

$$R(h) = \frac{\beta_{\mathrm{a}}(h) + \beta_{\mathrm{m}}(h)}{\beta_{\mathrm{m}}(h)},$$

where δ_{m} is the molecular depolarization ratio, whose value for dry air is assumed to be 0.28. β_{m} and β_{a} are the molecular and aerosol backscatter values. β_{m} for S channel, β_{ms} is computed as $\beta_{\mathrm{m}}{}^{*}$ 0.028 (Ref. 11). $R_{\mathrm{s}}(r)$ and $R_{\mathrm{p}}(r)$ are the effective backscatter ratio of the S and P channels, respectively. LR and LDR are the two important quantities in aerosol and cloud studies using lidar. These two parameters are important in the study of microphysical phase of the clouds and also useful for trace back the sources and sinks of the observed aerosols. The extinction-to-backscatter ratio, usually called as LR is an important parameter to obtain the nature of the scatterers while studying the optical properties of clouds and aerosols using lidar. The LR values in combination with LDR are used to suggest the type of ice crystals present in clouds. The altitude dependent LR value was calculated from the method described in detail by Satyanarayana et al.[12]

3.2 *MST Radar Data Analysis*

The complex time series of the decoded and integrated signal samples are fast Fourier transformed for online computation of the range dependent Doppler power. The data processing for parameterization of the Doppler spectrum involves the removal of bias, estimation of average noise level, incoherent integration, and computation of the three low order moments. For estimating the average noise level, an objective method developed by Hildebrand and Seckhon[13] has been adopted here. More details on this analysis are elaborately described by Rao et al.[6]

4 Experimental Observations

Lidar data collected during the period 2009 and 2010 are analyzed to estimate the various physical and microphysical properties of the cirrus clouds like cloud top, cloud base, optical depth, cloud depolarization ratio, LR, and cloud turbidity. The variability of cloud optical depth,

depolarization ratio, extinction, and LR with turbulence is studied using the lidar data. The lidar was operated on a continuous basis and 41 days of observations were made during the period 2009 to 2010. Out of these, cirrus cloud occurrence was noted on 28 days.

4.1 *Temporal Variation of Geometrical and Optical Properties of Cirrus*

The monthly variation of tropical cirrus properties are examined for those nights in which single layer cirrus persisted overnight. Lidar data are also studied to understand the seasonal variability. The four prominent seasons of the station are south-west monsoon (June, July, and August), north-east monsoon (September, October, and November), summer (March, April, and May), and winter (December, January, and February).

Clouds are then identified as cirrus according to two criteria. First, the cloud layer must be as cold as −25°C (Ref. 13). Second, the scattering ratio (SR), defined as the ratio of the total (molecular and particle) backscatter coefficient divided by the molecular backscatter coefficient, must be above a defined threshold. Threshold for a day is the average SR obtained for a certain range of height. The cloud is a region with sharp increase in SR. Cloud bottom is found from the height where the SR increases and the cloud top is the range at which the SR falls back to thresh hold value on that particular day.

Figure 1 shows the monthly variation of the cloud base and cloud top along with the tropopause height. It can be seen that the cirrus clouds have higher values of base height in the months of February, April, June, and October during the year 2009, with the highest value of base height observed in October. The cloud base has the lowest value in the month of August in 2009. For the year 2010, the cirrus clouds have high values of base height in the months of April and August. The observed values of cloud base are low for the month of March and October in 2010. It is observed that in the year 2009, the top height of cirrus clouds have high values in the month of February and October. The highest value of cirrus top height is observed in February. In 2010, the cirrus top height shows the highest value in the month of April and the lowest value in the month of March. The cloud top observed for the months February and October in 2009 lie closely to the tropopause. But for the year 2010, no cloud tops are seen near tropopause. Figure 1 shows large variation in the values of cloud base height for low altitude clouds. The variation in cloud base height for the cirrus clouds formed near to the tropopause is relatively less. It is interesting to note that low altitude cirrus clouds down to a height of 9 km were observed during the period July to September in 2009. These type of clouds were absent during the rest of the period.

The cloud geometrical thickness, defined as the full width at the half maximum of the profile; given in Fig. 2, shows the variation of percentage of occurrence of cirrus clouds of different geometrical thickness in the years 2009 and 2010. From Fig. 2(a), it can be seen that about 60% of the cirrus clouds formed are thin with geometrical thickness varying from 1 to 2 km. Only 7% of the clouds formed are very thick (thickness >4 km) for the year 2009. In the year 2010, about 77% of the total clouds formed are thin clouds having thickness 1

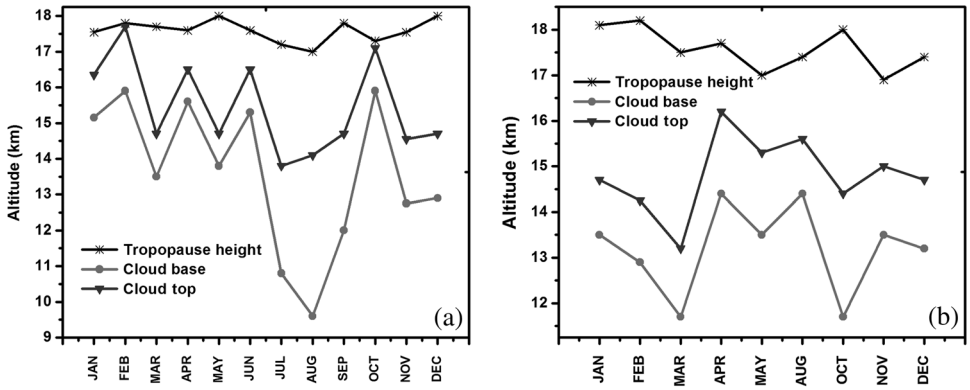

Fig. 1 Cloud base, cloud top, and tropopause height during the days of observation (a) 2009 and (b) 2010.

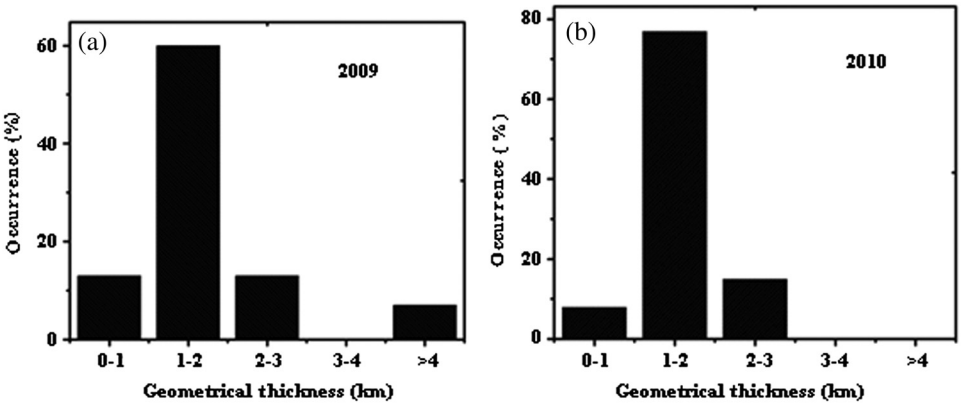

Fig. 2 The variation of percentage of occurrence of cirrus clouds of different geometrical thickness (a) for the year 2009 and (b) for the year 2010.

to 2 km as seen in Fig. 2(b). Interestingly, no thick clouds (thickness >3 km) are found for the year 2010. From these limited data observations, it can be found that most of the cirrus clouds formed is thin, with the thickness in the range of 1 to 2 km. This result is consistent with similar studies done at the same tropical station.[14]

Figures 3(a) and 3(b) show the percentage of occurrence of cirrus clouds as a function of midcloud altitude in the years 2009 and 2010. From Fig. 3(a), it can be seen that the occurrence of clouds is highest (~27%) at altitude range 15 to 16 km in the year 2009. But no clouds are observed in that altitude range in the year 2010. For the year 2010, the occurrence of cloud is the highest (~46%) at altitude range 13 to 14 km. For the year 2009, both the altitude ranges 12 to 13 and 13 to 14 km have recorded the same percentage of occurrence of the clouds (20% each). About 23% of the cloud occurrences is observed for both altitude ranges 11 to 12 and 14 to 15 km in the year 2010. It can also be seen that in the tropopause region where the temperature inversion take place (tropical tropopause layer), the occurrence of clouds is about 40% in 2009 and >50% in 2010. This is in agreement with the observations made by Sunilkumar et al.[15] at the same station.

Even though the limited data cannot show the seasonal behavior, a general trend could be seen by studying the data on a seasonal basis. The seasonal variation of the geometrical properties of the cirrus clouds for the year 2009 and 2010 is also shown in Fig. 4. From the seasonal observation, it is observed that the cloud top is the highest during the north-east monsoon in 2009 and during south-west monsoon in 2010. The cloud top height is lowest during winter 2009, whereas the cloud top height remains almost same during north-east monsoon and winter for 2010.

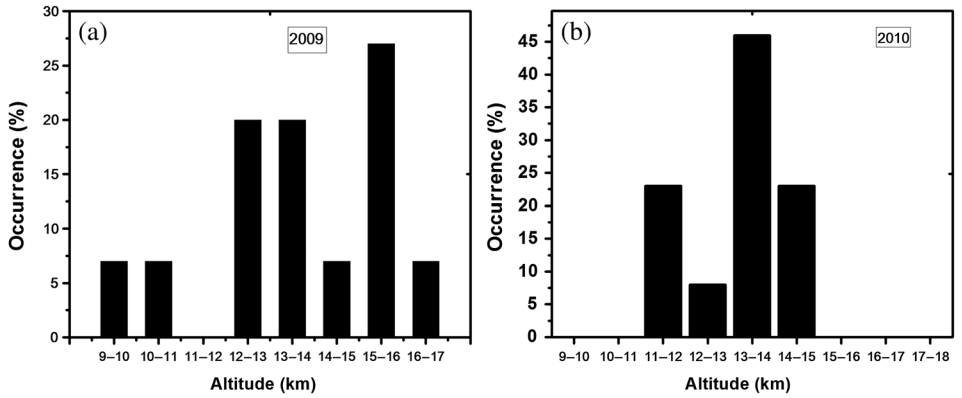

Fig. 3 The percentage of occurrence of cirrus clouds as a function of altitude (a) for the year 2009 and (b) for the year 2010.

Table 2 Seasonal geometrical thickness of clouds.

	Geometrical thickness of clouds (km)	
Season	2009	2010
Summer	1	1.7
South-west monsoon	2.9	1.2
North-east monsoon	1.9	2.1
Winter	1.45	1.5

From Fig. 4, it can be seen that the clouds are thin during summer and thicker during the south-west monsoon for the year 2009, which is the general pattern of clouds at this station. Extensive studies done by Parameshwaran et al.[10] and Sunilkumar et al.[14] support the argument. But for the year 2010, the clouds are thin during the south-west monsoon and thicker during the north-east monsoon. A change from the normal pattern is found during this year. The seasonal variation of geometrical thickness of the clouds for the years 2009 and 2010 is given in Table 2.

Figure 5 shows a contour plot of the monthly evolution of volume depolarization ratio. It is worth to note that during the monsoon period, the upper troposphere is densely dominated by cirrus clouds originating from convective anvils.[16] The particle associated with the cirrus clouds will be large and nonspherical ice, which contribute to significantly large volume depolarization ratio.[17] The depolarization ratio profiles in Fig. 5 shows the three layer cirrus models proposed

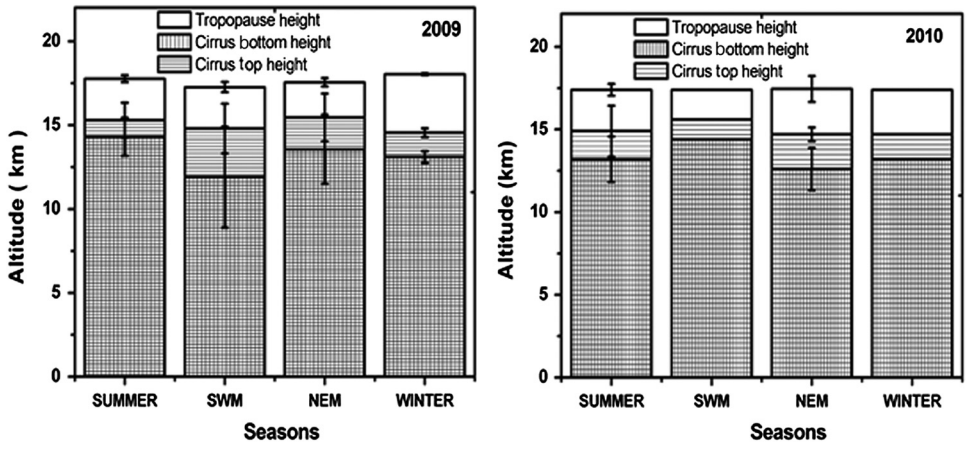

Fig. 4 The seasonal variation of the geometrical properties of the cirrus clouds for the year 2009 and 2010.

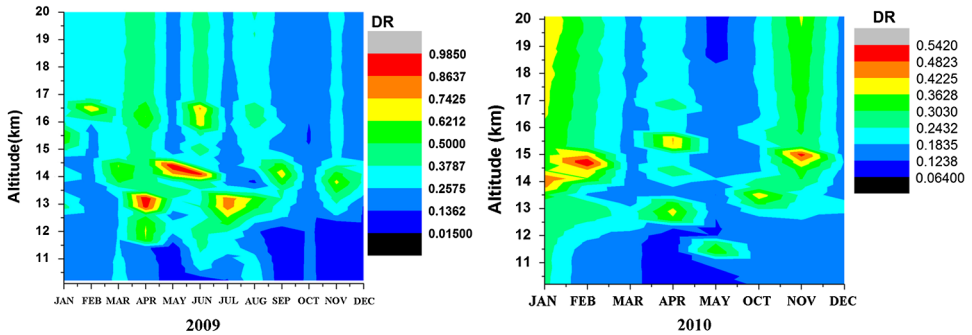

Fig. 5 Contour plot of the monthly evolution of depolarization ratio of cirrus clouds observed during the year 2009 and 2010.

by Heymsfield et al.[18] As per the model, the uppermost part is the nucleation layer. In this nucleation layer, the relative humidity exceeds the required level for ice nucleation and hence composed of small ice crystals. The middle layer of cirrus is called the growth layer. The growth layer has the physical conditions for crystal growth. The ice crystals grow from tens of microns to hundreds of microns in this layer. The lower most layers are the sublimation layer, where the ice crystals in the above layer fall into the dry air. This process lowers the cloud base and moistens the air below the clouds. The moistening of air below the cirrus cloud modifies the microphysical properties of aerosols in this region. This is manifested in the volume depolarization ratio. The volume depolarization ratio below the cloud is usually high. The high depolarization values during the period April–September is due to the presence of DC clouds. The profile in Fig. 5 shows a strong enhancement of volume depolarization ratio during June–July (2009). This period is highly convective with convection near Bay of Bengal attaining peak altitude.[19] Frequent penetration of cirrus clouds into tropopause is also observed during this period. This is in line with the previous observations made from the same station.[20] The 2010 depolarization profiles show slight anomaly with respect to the observations made in 2009. This anomaly during 2010 was evident when compared with the similar previous observation from the station. The 2010 profiles are found to have less depolarization ratios at the cloud center when compared to that of the year 2009. Figure 6 shows the variation of depolarization ratio with altitude for years 2009 and 2010. Majority of clouds in 2009 have depolarization ratio >0.3, indicating the presence of hexagonal ice crystals. High altitudes clouds with depolarization ratios <0.3, indicate the presence of horizontally oriented ice crystals or thin plates of ice crystals. Most of the clouds in 2010 except those in higher altitudes, show depolarization ratio <0.3, indicating most of the clouds consist of horizontally oriented ice crystals or thin plates of ice crystals. The clouds lying in the altitude range 13 to 15 km have comparatively higher depolarization ratio signifying the presence of hexagonal ice crystals. Tables 4 and 5 summarize the physical, optical, and morphological parameters of the cirrus clouds observed in 2009 and 2010. LR depends on the properties of ice crystals. Heymsfield and Platt[15,21] has revealed that many types of ice crystals exist inside the cirrus clouds with the temperatures $\leq -50°C$. This temperature gradient is usually observed around 12 km in the tropics.

Satyanaryana et al.[12] have developed a method to derive the range dependent LR. By this method, it was found that the LR at cloud bottom and cloud top is higher than that of the cloud midpoint. The LR varied randomly below 12.5 km and above 12.5 km, the LR (S) values are usually in the range 20 to 40. The method developed by Satyanaryana et al. does not consider the effect due to multiple scattering. From the computed values of LR, information about multiple scattering can be obtained. The contour plots for the monthly mean LR for the years 2009 and 2010 are given in Fig. 7.

The calculated values of the LRs for the years 2009 and 2010 are given in Tables 4 and 5. The calculated values are consistent with the values reported by Platt et al.[22] and Sassen and Cho[23] The value of extinction coefficient, LR, and depolarization ratio together can be used to get more information regarding the morphology of ice crystals formed. Sassen and Cho[23] have given

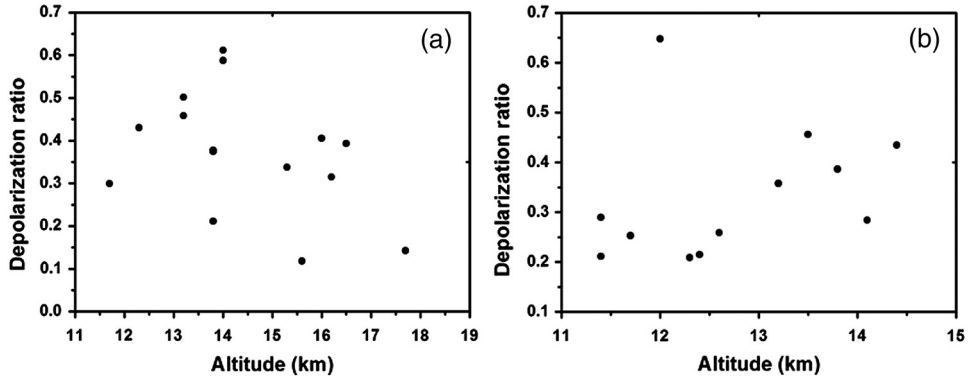

Fig. 6 Variation of depolarization ratio with respect to altitude (a) 2009 and (b) 2010.

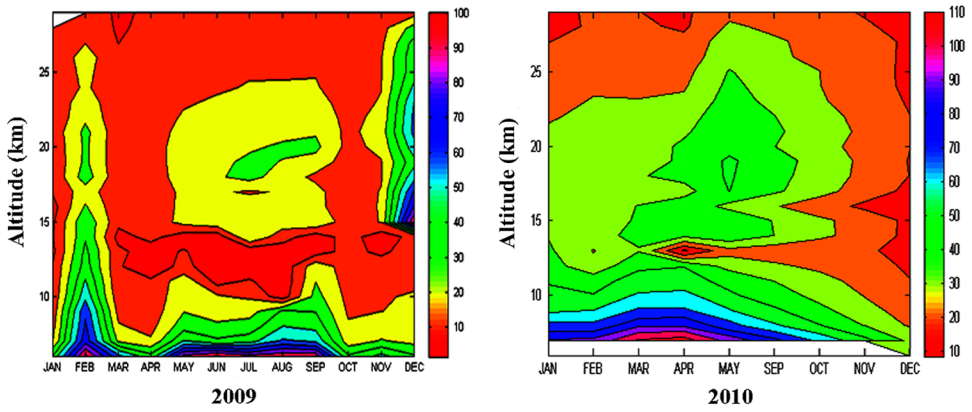

Fig. 7 The contour plot of the monthly variation of lidar ratio (LR) of cirrus clouds observed in the year (a) 2009 and (b) 2010.

a classification of hexagonal ice crystals based on the values of LR and the depolarization ratio (Table 3).

Based on the classification given by Sassen and Cho, the shape of the ice crystals in the clouds is identified and is presented in Tables 4 and 5. The ice habit classification based on 1 day average does not give much insight as shapes of ice crystals changes with temporal and spatial variability of microphysics. However, the current prediction cannot tell about the ice crystal morphology at a large time scale, it will certainly give a good insight of crystal morphology at the time of the lidar measurement. The temperature data are obtained from the radio sonde measurements, with collocated instruments at the same period of lidar observation.

4.2 *Measure of Turbulence Using a Static Model and with a Dynamic Real-Time Monitoring Using MST Radar*

Turbulent mixing in atmosphere creates local changes in temperature, humidity, and atmospheric composition, which can lead to changes in the index of refraction. Turbulence occurs in all three velocity components (zonal, meridional, and vertical) and is unpredictable; however, statistically distinct properties of the turbulence can be identified and analyzed. Turbulence exhibits a broad range of spatial and temporal scales resulting in efficient mixing of fluid properties. Turbulence is important because it mixes and churns the atmosphere and causes water vapor, smoke, and other substances, as well as energy, to become distributed both vertically and horizontally. In this study, the effect of turbulence in cirrus ice crystal formation is studied by computing the refractive index structure parameter C_n^2. C_n^2 is derived by using the dynamical vertical wind component from the MST radar data. The refractive index structure parameter C_n^2 is calculated by using one of the most used models; Hufnagel-Valley,[24] defined by the following equation:

$$C_n^2 = 0.00594\left(\frac{v}{27}\right)^2 (10^{-5}h)^{10}\exp\left(\frac{-h}{1000}\right) + 2.7\times 10^{-16}\exp\left(\frac{-h}{1500}\right) + A_0\exp\left(\frac{-h}{100}\right),$$

Table 3 Types of hexagonal crystals and their LR and DR.

Crystal types	Lidar ratio	Depolarization ratio
Hexagonal thin plates	38.5	0.4
Hexagonal thick plates	11.6	0.5
Hexagonal long column	26.3	0.6

Table 4 Optical properties of cirrus clouds over Gadanki station during the period 2009.

Date of observation	CBH (km)	CTH (km)	*T* (km)	CMH (km)	Temp (K)	DR	Extinction (m^{-1})	OD (m)	LR	Morphology of crystals predicted
January 21, 2009	15.6	16.8	1.2	16.2	195	0.31	3.43E – 06 to 2.96E – 06	0.010	12-3-1 1	Hexagonal thick plates
January 28, 2009	14.7	15.9	1.2	15.3	200	0.34	4.04E – 06 to 2.71E – 06	0.028	9-9-3	Hexagonal thick plates
February 11, 2009	15.9	17.1	1.2	16.5	188	0.39	1.02E – 05 to 7.04E – 06	0.027	32-16-57	Hexagonal thin plates
March 4, 2009	13.5	14.7	1.2	14.0	211	0.61	4.96E – 06 to 4.22E – 06	0.019	19-4-20	Hexagonal long columns
April 1, 2009	15.6	16.5	1	16	199	0.40	4.44E – 06 to 3.61E – 06	0.025	7-4-7	Hexagonal thick plates
May 13, 2009	13.8	14.7	0.9	14	211	0.58	6.49E – 06 to 3.45E – 06	0.019	20-3-10	Hexagonal long columns
June 3, 2009	11	15	3	13.2	199	0.46	1.14E – 05 to 3.45E – 06	0.244	26-2-14	Hexagonal long columns
July 22, 2009	10.8	13.6	2-8	12.3	236	0.43	8.18E – 06 to 3.38E – 06	0.066	22-2-9	Hexagonal long columns
August 5, 2009	9.6	14.0	4.4	11.7	245	0.30	1.19E – 05 to 1.09E – 05	0.383	12-6-32	Thin plates/oriented other type of crystals
September 16, 2009	12	14.4	2.4	13.8	224	0.38	4.35E – 06 to 3.77E – 06	0.465	14-4-26	Hexagonal thick plate
October 7, 2009	16.8	18	1.2	17.7	193	0.14	2.35E – 06 to 2.22E – 06	0.004	12-11-13	Oriented other type of crystals
October 21, 2009	15	16.2	1.2	15.6	199	0.12	2.99E – 06 to 2.58E – 06	0.005	14-9-14	Thin plates
November 18, 2009	12.3	14.4	2.1	13.2	221	0.50	5.34E – 06 to 4.29E – 06	0.064	24-1-20	Hexagonal long column
November 25, 2009	13.2	14.7	1.5	13.8	214	0.37	3.64E – 06 to 3.04E – 06	0.012	13-4-12	Hexagonal thick plate
December 30, 2009	12.9	14.7	1.8	13.8	215	0.21	5.53E – 06 to 3.25E – 06	0.063	12-8-12	Thin plates/oriented other type of crystals

Table 5 Optical properties of cirrus clouds over Gadanki station during the period 2010.

Date	CTH (km)	CBH (km)	CMH (km)	*T* (km)	Temp (K)	DR	Extinction (m^{-1})	OD (m)	LR (CT-CM-CB)	Morphology of crystals predicted
January 6, 2010	14.7	13.8	14.1	0.9	209	0.39	2.87E – 05 to 2.99E – 05	0.042	38-10-24	Hexagonal long column
January 13, 2010	14.4	13.2	13.8	1.2	212	0.36	3.06E – 05 to 3.49E – 05	0.163	44-44-47	Hexagonal thin plate
February 3, 2010	13.5	11.4	12.9	2.1	228	0.29	1.566E – 05 to 2.97E – 05	0.427	39-5-42	Hexagonal thin plate
February 10, 2010	15.3	14.4	14.7	0.6	211	0.43	2.72E – 05 to 5.53E – 05	0.256	22-5-38	Hexagonal thin plates
February 17, 2010	15	13.5	14.8	1.5	169	0.46	1.95E – 05 to 2.83E – 05	0.227	31-10-31	Hexagonal thin plates
March 17, 2010	13.2	11.7	12.6	1.5	224	0.25	2E – 05 to 2.93E – 05	0.300	36-10-37	Thin plates/oriented oilier type of crystals
April 28, 2010	13.5 (HALC)	12.4	12.9	1.1	206	0.21	1.53E – 05 to 2.54E – 05	0.478	16-5-39	Thin plates/oriented other type of crystals
May 12, 2010	13 8 (HALC)	12.0	13.3	1.8	214	0.65	1.368E – 05 to 4.899E – 05	0.633	18-11-46	Hexagonal long column
August 11, 2010	15.6 (HALC)	14.4	15.1	1.2	207	(S comp noisy)	1.16E – 05 to 8.08E – 05	0.769	21-8-32	
October 13, 2010	14.1	11.4	13.5	2.7	227	0.21	3.22E – 05 to 3.1E – 05	0.778	30-5-9	Thin plates/oriented other type of crystals
November 19, 2010	15.1	12.6	14.7	2.5	210	0.26	2.12E – 05 to 5.17E – 05	0.752	31-5-8	Thin plates/oriented other type of crystals
December 22, 2010	16.2	14.1	15	2.1	205	0.28	2.2E – 05 to 3.27E – 05	0.112	22-6-10	Thin plates/oriented other type of crystals
December 31, 2010	13.5	12.3	12.9	1.2	220	0.21	1.97E – 05 to 3.22E – 05	0.259	10-7-25	Thin plates/oriented other type of crystals

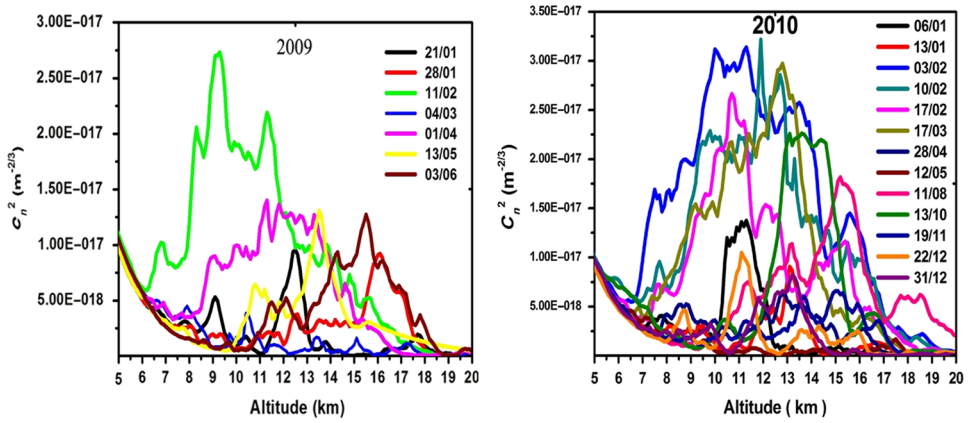

Fig. 8 Turbulence as a measure of refractive index (C_n^2) for the period 2009 and 2010.

where h is the altitude in (m), v is the wind speed at high altitude (m/s) (obtained from GPS sonde measurement made from the station), and A_0 is the turbulence strength at ground level, $=1.7 \times 10^{-14}$ $m^{-2}/3$.

The turbulence profile is generated by using the vertical wind velocity derived from GPS sonde measurement done during the same time of lidar observation with the instrument colocated at the station. High turbulence is found during the days of February for both 2009 and 2010. For the rest of the days in 2009, relatively lower turbulence values were observed. The year 2010 had moderately high values of turbulence observed for all days of observation except during winter. The altitude range 8 to 12 km shows the high values of turbulence during the year 2009. Above 12 km, the value of turbulence is relatively less for the year. The year 2010 had relatively higher turbulence for an altitude range 8 to16 km. High level of turbulence is likely to occur during the monsoon periods due to the large convection activities like inter tropical convergence zone prevailing in the geographical region. Particularly, the deep convection near the Head Bay of Bengal attains its peak altitude, during the period June–July.[20] The C_n^2 profiles in Fig. 8 were from the static Hufnagel-Valley model. As few observations were only possible, the results cannot be endorsed on a seasonal scale. To compare the static model value with a dynamical experimental value, MST radar collocated at the lidar facility was employed. MST radar data were obtained for the same days for which the turbulence study was conducted. The study shows a similar trend for the above discussed days with more dynamic variability.

4.3 *Effect of Turbulence in Cloud Microphysics*

The effect of turbulence in extinction, LR, and depolarization ratio is discussed in Figs. 9 and 10. Four days of near simultaneous observation of LR, extinction coefficient, depolarization ratio, and turbulence were taken for the study from the period 2009 to 2010. Out of the four days two turbulent days and turbulence free days are selected for the study.

Figures 10 and 11 show the negative correlation between the LR and extinction inside a cloud structure. The extinction coefficient increases inside the cloud near the cloud center and the LR decreases inside the same region of the cloud. The depolarization value also increases inside the cloud. The region of cloud which has more ordered crystals has high depolarization value. It is clearly seen that the turbulence has direct effect on the symmetric nature of the clouds. The clouds appear to be more asymmetric in nature with the presence of turbulence in the cloud region. The depolarization ratio is found to be high in the cloud region where the turbulence effect is high. This predicts the possibility of formation of ordered crystals with turbulence. Ordered crystals in the clouds give rise to high depolarization ratio. The crystal growth is increased in regions of high turbulence. This in turn rapidly reduces the LR. The rapid decrease in LR inside the clouds, with values <9 suggest formation of large crystals. The increase in turbulence coincides with the spread in the Hadley vortex toward the both side of equator that takes place in this height. Turbulence is very high at this altitude (10 to 15 km) at the tropics. But in the case of high altitude clouds above the tropopause layer, there is no significant increase

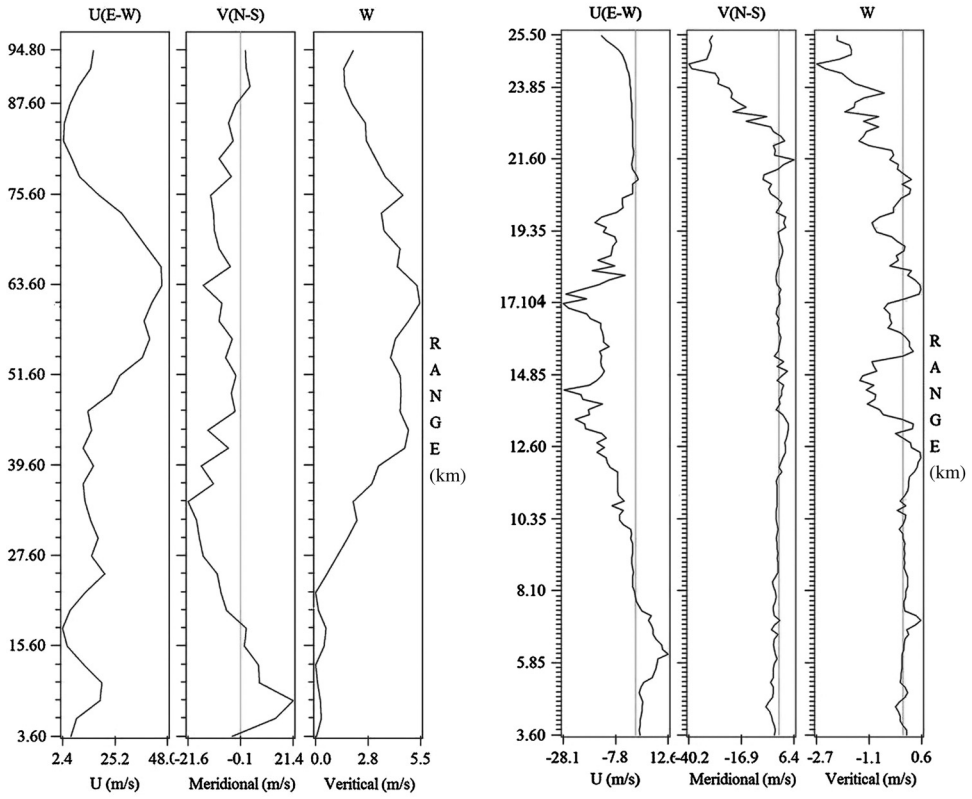

Fig. 9 (a) The vertical wind profile on a less turbulent day 11/02/2009 and (b) 13/10/2010.

in optical depth. This is because the turbulence, here, is generated by means of oscillations like the Brewer Dobson circulation,[25,26] which exist above the tropopause layer.

5 Turbulence and Cloud Asymmetry

It is seen that the cloud back SR varies significantly in altitude with high values in the middle and low values toward the upper peripheries. A typical plot of extinction coefficient profile (for 4 March 2009) is shown in Fig. 12. From the Figs. 10 and 11, it can be seen that the geometric center of the cloud and the altitude corresponding to the peak value of extinction coefficient do not coincide. This means that the extinction coefficient profile within the cloud is not perfectly in Gaussian in shape. In other words, as far as scattering is concerned, the cloud is neither homogeneous nor optically symmetric with respect to its center. The degree of deviation from the symmetric nature of the extinction coefficient profile of the cloud can be determined in terms of the factor ξ.[27] ξ of the cloud is defined by the following equation:

$$\xi = \frac{(h_{\mathrm{m}} - h_{\mathrm{cb}})}{(h_{\mathrm{ct}} - h_{\mathrm{cb}})},$$

where h_{m} is the optical midcloud height, h_{cb} is the cloud base altitude, and h_{ct} is the cloud top altitude.

If the extinction profile within the cloud is Gaussian, the value of ξ will be around 0.5. If the value of ξ is <0.5, the scattering will be more from the lower half of the cloud and if ξ is >0.5, the scattering will be more from the upper half of the cloud. The amount of asymmetry could be quantified in terms of its absolute deviation from 0.5. The asymmetric factor ξ for the cirrus clouds observed during the years 2009 and 2010 is computed and presented. From Fig. 13, it can be seen that the cirrus cloud extinction seems to be almost symmetric during the entire period of the year 2009 except in the beginning of the north-east monsoon, whereas during the entire period of 2010, the cloud shows asymmetric nature. During the year 2010, the value of the ξ shows high values and this suggests the cloud has high scattering from the upper portion.

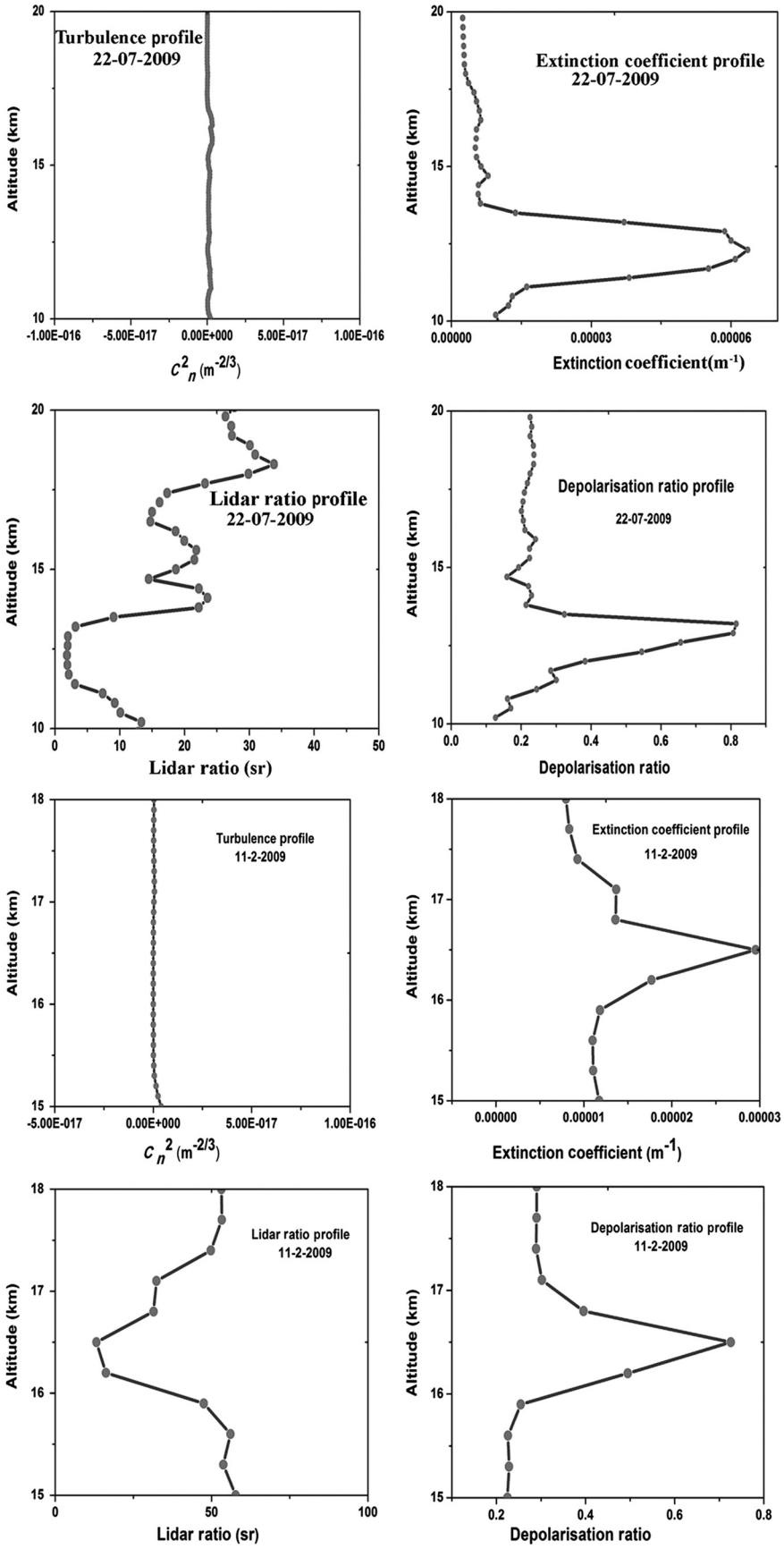

Fig. 10 Profiles of turbulence, extinction, LR, and depolarization ratio for a nonturbulent day.

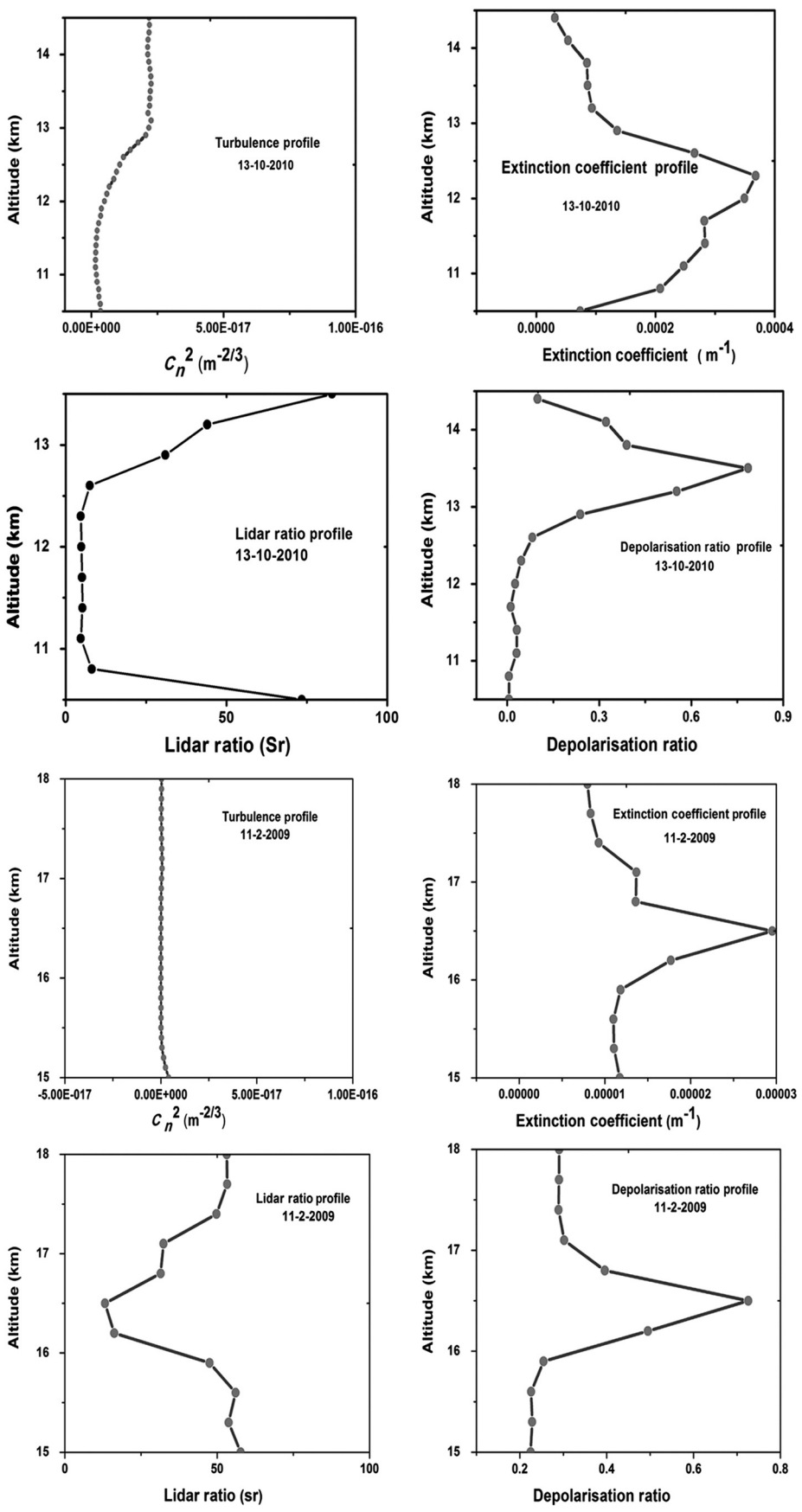

Fig. 11 Profiles of turbulence, extinction, LR, and depolarization ratio for a turbulent day.

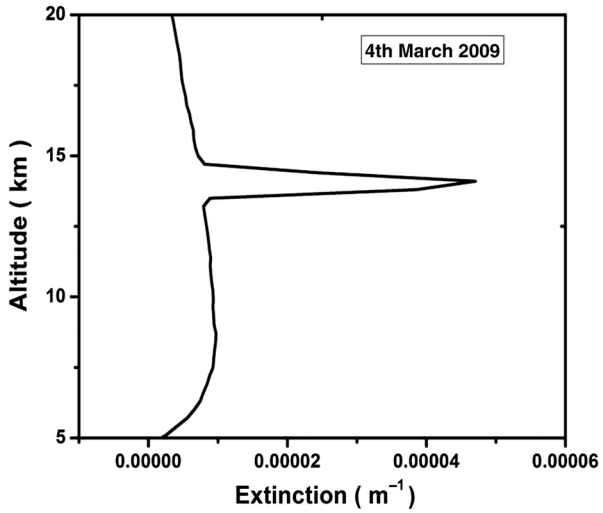

Fig. 12 A typical plot of extinction coefficient profile (for March 4, 2009).

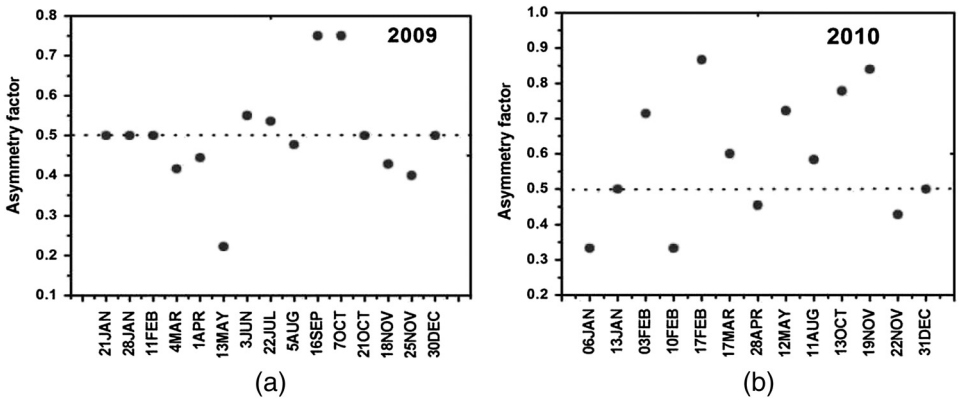

Fig. 13 Scatter plot of the asymmetry factor for cirrus clouds on different days (a) observed in 2009 and (b) observed in 2010.

Figure 14 shows scattered plot for the factor ξ of the cirrus clouds as a function of altitude for the period 2009 to 2010. Clouds detected in 2009 are found to be symmetric for all altitude of occurrence, with a few exceptions at altitudes 14 and 18 km. In 2010, clouds observed are asymmetric with ξ varying widely from the normal value of 0.5 and there is no particular altitude where symmetry is restored. Figure 15 shows the variation of asymmetric nature of cloud extinction as a function of geometrical thickness of the clouds.

Cloud asymmetry during 2010 can be associated with the moderately high turbulence that existed in that period. High atmospheric turbulence facilitates rapid ice nucleation and it is accounted with the presence of large ice content observed during 2010. Due to rapid cooling, crystalline ice can form in any part of a cloud. This will shift the Gaussian peak away from the geometrical center. This shift will create asymmetry in its shape. The asymmetric clouds are found to be multiscattering. The multiple scattering factor $\eta_{(z)}$ is obtained from the optical depth τ_c by the following equation:

$$\eta = \frac{D}{\int_0^D e^{\tau_c(h)} \mathrm{d}h} = \frac{\tau_c}{e^{\tau_c} - 1},$$

where D is the physical thickness of the cloud and h is the laser penetration depth. For smaller values of optical depth, $\eta(z) \approx 1$. When the multiple scattering effects is negligible, $\eta(z) = 1$.

Smaller values of $\eta(z)$ correspond to larger multiple scattering effects.

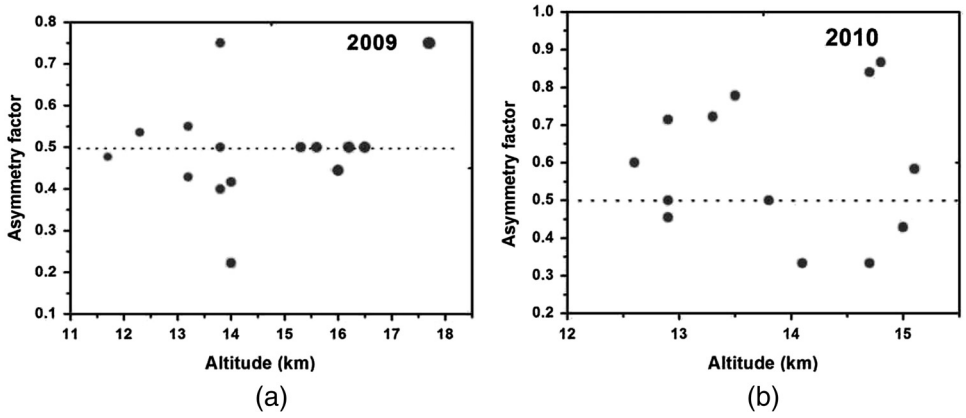

Fig. 14 Scatter plot for the asymmetric factor of the cirrus clouds as a function of altitude (a) 2009 and (b) 2010.

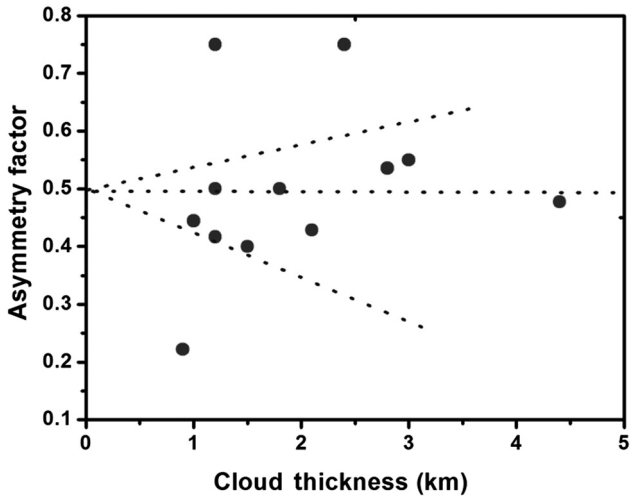

Fig. 15 Scatter plot showing the dependence of cloud asymmetry factor (ξ) on cloud geometric thickness during 2009.

Scatter plot showing the multiple scattering factor (η) for different days of observations in 2009 and 2010 is given in Fig. 16. The above findings predict some anomaly that may have occurred during 2010, which might have caused the occurrence of abnormal TC clouds during south-west monsoon, clouds with low depolarization values at the cloud center, high turbidity, more asymmetric clouds, and more multiscattering clouds. Extensive data would have consolidated the findings.

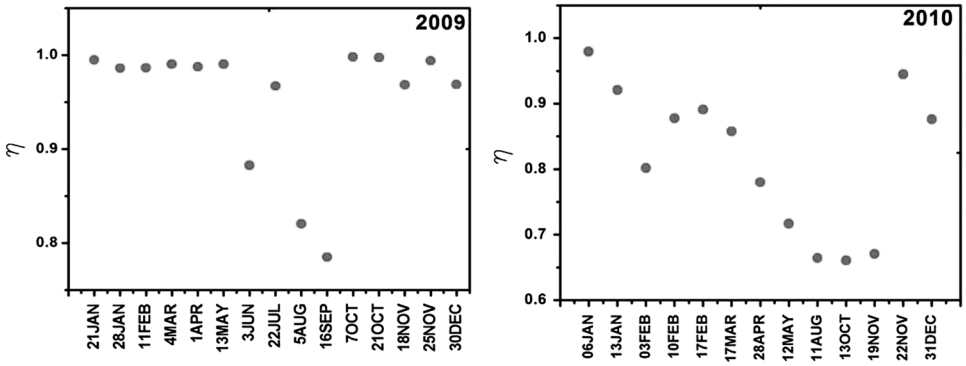

Fig. 16 Scatter plot showing the multiple scattering factor (η) for the observation periods 2009 and 2010.

6 Conclusion

The study discusses the formation, geometrical, and microphysical properties of cirrus clouds observed from the station during the period 2009 to 2010. Even though the work does not have extensive data, general seasonal trends in optical and microphysical properties have been discussed. Cloud height values show a maximum occurrence in the narrow 13 to 14 km range. The cloud average thickness derived from the lidar system is 1.5 km for a temperature range −17°C to −87°C with extinction coefficient in the range 6.8×10^{-4} to 1.6×10^{-4} m^{-1}. There are considerable differences in the properties obtained among 2009 and 2010 showing significant anomalous behavior in 2010. The clouds observed during 2010 show relatively high asymmetry and large multiple scatterings. Turbulence computed using the static Hufnagel-Valley model and MST radar data explains the dependence of turbulence and ice nucleation, turbulence, and cloud asymmetry. The case study done for turbulent and nonturbulent days states the negative correlation between the LR and extinction inside a cloud structure.

It is also observed that the depolarization ratio is found to be high in the cloud region where the turbulence effect is high. The study suggests the possibility of formation of ordered crystals with turbulence. Ordered crystals give rise to high depolarization ratio with reduced LR.

The findings suggest that the anomaly of physical and optical properties of cirrus observed from the station in 2010 has certain relation with dynamical variability like turbulence. The dynamical variability like convective contrails, Indian Ocean dipole moment will certainly modify the properties of the cirrus occurring in the region. Extensive lidar data supported with meteorological data from land and sea covering, larger grid can certainly prove their effects.

Acknowledgments

The authors thank the National Atmospheric Research Laboratory, Department of Space, Government of India, Gadanki, Tirupati, India and ISRO-RESPOND for providing the facility, data, and financial support for this work.

References

1. G. G. Mace et al., "Cloud radiative forcing at the atmospheric radiation measurement program climate research facility: 1. Technique, validation, and comparison to satellite-derived diagnostic quantities," *J. Geophys. Res.* **111**, D11S90 (2006), http://dx.doi.org/10.1029/2005JD005921.
2. K. N. Liou, "Influence of cirrus clouds on weather and climate processes: a global perspective," *Mon. Weather Rev.* **114**(6), 1167–1192 (1986), http://dx.doi.org/10.1175/1520-0493(1986)114<1167:IOCCOW>2.0.CO;2.
3. R. E. Good et al., "Atmospheric models of optical turbulence," *Proc. SPIE* **928**, 165–186 (1988).
4. R. R. Beland, "Propagation through atmospheric optical turbulence," in *The Infrared and Electro-Optical Systems Handbook*, Vol. 2, pp. 161–211, Infrared Information Analysis Center, Environmental Research Institute of Michigan, SPIE Optical Engineering Press, Bellingham, Washington (1993).
5. Y. Bhavanikumar, C. NageswaraRaju, and M. Krishnaiah, "Indo-Japanese, Lidar observations of the tropical middle atmosphere during 1998 and 1999," *Adv. Atmos. Sci.* **23**(5), 711–725 (2006), http://dx.doi.org/10.1007/s00376-006-0711-0.
6. P. B. Rao et al., "Indian MST radar 1. System description and sample vector wind measurements in ST mode," *Radio Sci.* **30**(4), 1125–1138 (1995), http://dx.doi.org/10.1029/95RS00787.
7. F. D. Fernald, "Analysis of atmospheric lidar observations: some comments," *Appl. Opt.* **23**(5), 652–653 (1984), http://dx.doi.org/10.1364/AO.23.000652.
8. M. N. Sasi and K. Sengupta, "A reference atmosphere for Indian equatorial zone from surface to 80 km," Scientific Report SPL: SR: 006:85, Space Physics Laboratory, Vikram Sarabhai Space Centre, Kerala, India (1985).

9. K. Sassen and B. S. Cho, "Subvisual thin cirrus lidar data set for satellite verification and climatological research," *J. Appl. Meteorol.* **31**(11), 1275–1285 (1992), http://dx.doi.org/10.1175/1520-0450(1992)031<1275:STCLDF>2.0.CO;2.
10. K. Parameswaran et al., "Lidar observations of cirrus cloud near the tropical tropopause: temporal variations and association with tropospheric turbulence," *Atmos. Res.* **69**(1–2), 29–49 (2003), http://dx.doi.org/10.1016/j.atmosres.2003.08.002.
11. B. A. Bodhaine et al., "On Rayleigh optical depth calculations," *J. Atmos. Ocean. Technol.* **16**(11), 1854–1861 (1999), http://dx.doi.org/10.1175/1520-0426(1999)016<1854:ORODC>2.0.CO;2.
12. M. Satyanarayana et al., "Laser radar characterization of atmospheric aerosols in the troposphere and stratosphere using range dependent lidar ratio," *J. Appl. Remote Sens.* **4**(1), 043503 (2010), http://dx.doi.org/10.1117/1.3306573.
13. L. Goldfarb et al., "Cirrus climatological results obtained from lidar measurements at OHP (440N, 60E)," *Geophys. Res. Lett.* **28**(9), 1678–1690 (2001), http://dx.doi.org/10.1029/2000GL012701.
14. S. V. Sunilkumar et al., "Lidar observations of cirrus clouds near the tropical tropopause," *Atmos. Res.* **66**(3), 203–207 (2003), http://dx.doi.org/10.1016/S0169-8095(02)00159-X.
15. S. V. Sunilkumar, K. Parameswaran, and B. V. Thampi, "Interdependence of tropical cirrus properties and their variability," *Ann. Geophys.* **26**, 413–429 (2008), http://dx.doi.org/10.5194/angeo-26-413-2008.
16. S. V. Sunilkumar et al., "Semitransparent cirrus clouds in the tropical tropopause layer during two contrasting seasons," *J. Atmos. Solar-Terr. Phys.* **72**(9–10), 745–762 (2010), http://dx.doi.org/10.1016/j.jastp.2010.03.020.
17. B. V. Thampi, S. V. Sunilkumar, and K. Parameswaran, "Lidar studies of particulates in the UTLS region at a tropical station over the Indian subcontinent," *J. Geophys. Res.* **114**, D08207 (2009), http://dx.doi.org/10.1029/2008JD010556.
18. G. M. Mc Farquhar, A. J. Heymsfield, and B. Hart, "Midlatitude and tropical cirrus—microphysical properties," in *Cirrus*, D. Lynch et al., Eds., pp. 78–101, Oxford University Press, New York (2002).
19. S. Meenu, K. Rajeev, and K. Parameshwaran, "Regional and vertical distribution of semitransparent cirrus clouds and cloud top altitudes over tropical Indian region derived from CALIPSO data," *J. Atmos. Solar-Terr. Phys.* **73**(13), 1967–1979 (2011), http://dx.doi.org/10.1016/j.jastp.2011.06.007.
20. S. Meenu et al., "Regional and vertical distribution of deep clouds and cloud top altitudes over the Indian subcontinent and the surrounding oceans," *J. Geophys. Res.* **115**, D05205 (2010), http://dx.doi.org/10.1029/2009JD011802.
21. A. J. Heymsfield and C. M. R. Platt, "A parameterization of the particle size spectrum of ice clouds in terms of ambient temperature and their ice water content," *J. Atmos. Sci.* **41**(5), 846–855 (1984), http://dx.doi.org/10.1175/1520-0469(1984)041<0846:APOTPS>2.0.CO;2.
22. C. M. R. Platt, J. C. Scott, and A. C. Dilley, "Remote sounding of high clouds VI: optical properties of mid latitude and tropical cirrus," *Atmos. Sci.* **44**(4), 729–747 (1987), http://dx.doi.org/10.1175/1520-0469(1987)044<0729:RSOHCP>2.0.CO;2.
23. K. Sassen and B. S. Cho, "Sub visual thin cirrus lidar data set for satellite verification and climatological research," *J. Appl. Meteorol.* **31**(11), 1275–1285 (1992), http://dx.doi.org/10.1175/1520-0450(1992)031<1275:STCLDF>2.0.CO;2.
24. L. W. William and G. J. Zissis, "Propagation through atmospheric turbulence," in *The Infrared Handbook*, Infrared Information Analysis Center, Ann Arbor, MI (1985).
25. D. Rind and W. B. Rossow, "The effects of physical process on the Hadley cell," *J. Atmos. Sci.* **41**(4), 479–507 (1984), http://dx.doi.org/10.1175/1520-0469(1984)041<0479:TEOPPO>2.0.CO;2.
26. S. J. Eichelberger and D. L. Hartmann, "Changes in the strength of the Brewer–Dobson circulation in a simple AGCM," *Geophys. Res. Lett.* **32**, L15807 (2005), http://dx.doi.org/10.1029/2005GL022924.
27. E. W. Eloranta, "Practical model for the calculation of multiply scattered lidar returns," *Appl. Opt.* **37**(12), 2464–2472 (1998), http://dx.doi.org/10.1364/AO.37.002464.

Vasudevannair Krishnakumar obtained his MSc degree in physics from Mahatma Gandhi University, Kerala, in 2002, an MPhil degree in photonics from the Department of Optoelectronics, University of Kerala, in 2004, and a PhD degree in applied science and technology from the Department of Optoelectronics, University of Kerala, Trivandrum, India, in 2013. He is now working as an associate professor at Mohandas College of Engineering and Technology, Trivandrum, India. His fields of interest are LIDAR studies on atmospheric aerosols and clouds.

Malladi Satyanarayana obtained his MSc (Tech.) and PhD in applied physics from Andhra University, India. He joined Vikram Sarabhai Space Centre (VSSC), Trivandrum, in 1972 and had been working in the Space Physics Laboratory, VSSC. He was the head of the Atmospheric LIDAR's Branch in Space Physics Laboratory, VSSC, and also was the project director of Space Borne LIDAR Project of ISRO. Presently, he is working as a visiting professor in the Department of Optoelectronics, University of Kerala, Kariavattom, Trivandrum, Kerala, India.

Soman R. Radhakrishnan received his MSc degree in physics and an MPhil degree in photonics from the University of Kerala in 2003 and 2006, respectively. He obtained his PhD from Department of Optoelectronics, University of Kerala. He is currently working as a scientist at National Physical Laboratory, New Delhi.

Reji K. Dhaman acquired an MSc degree in physics and an MTech degree in electronics and communication optoelectronics and optical communication from the University of Kerala in 2004 and 2009, respectively. He is working as a junior research fellow in the ISRO RESPOND project on aerosol, cloud, and water vapor precipitation effects on monsoon over the Indian subcontinent using LIDAR techniques from 2010 October onwards.

Glory Selvan Jayeshlal has acquired an MSc degree in physics and an MPhil degree in photonics from the University of Kerala. He is a full-time research scholar in the Department of Optoelectronics, University of Kerala, Kariavattom, Trivandrum, India. His current fields of interest are LIDAR and radar data analysis, and influence of aerosol on clouds.

Gopinathan Nair S. Motty has acquired an MSc degree in physics and an MPhil degree in photonics from the University of Kerala. She is a full-time research scholar in the Department of Optoelectronics, University of Kerala, Kariavattom, Trivandrum, India. Her current fields of interest are LIDAR data analysis and LIDAR inversion algorithm development.

Vellara P. Mahadevan Pillai has an MSc degree in physics, an MPhil degree in physics, and a PhD degree in laser Raman spectroscopy from Kerala University. Presently, he is working as professor and head of the Department of Optoelectronics, University of Kerala.

Karnam Raghunath is working as a scientist/engineer at the National Atmospheric Research Laboratory, Department of Space, Government of India, Tirupati, India, in the field of optical remote sensing area with atmospheric LIDARs. He has his bachelor of technology degree in electronics and communication engineering from Nagarjuna University, AP, India, and subsequently his master of engineering in communication systems from Regional Engineering College, Trichy, India. He has worked in the field of high power RF systems related to atmospheric radars while at the Society for Applied Microwave Electronics Engineering and Research, Mumbai, India.

Madineni Venkat Ratnam is a scientist at the National Atmospheric Research Laboratory (NARL), Department of Space, Government of India. He worked as postdoctoral fellow, scientist, and visiting scientist at Taiwan, Germany, and Japan, respectively, during 2001 to 2006. He has carried out several research projects sponsored by Government of India funding agencies like ISRO, DST, etc. He is specialized in the area of middle atmospheric structure and dynamics using novel GPS RO, GPS radiosonde, and MST radar techniques.

Duggirala Ramakrishna Rao graduated in engineering (BE in ECE) from Government College of Engineering, Kakinada, and completed postgraduation (MTech in EIE) from Regional

Engineering College, Warangal. He has vast experience in the fields of image processing, remote sensing, and LIDARs. He has published about 40 technical papers at the national and international level journals and conferences. He worked for ISRO about 35 years.

Pindlodi Sudhakar graduated in engineering (BTech in ECE) from DVR College of Engineering and Technology and postgraduation in engineering (MTech in ECE) from Mahaveer Institute of Science and Technology, both affiliated to JNTU, Hyderabad. He has about a decade of teaching and R&D experience. His areas of interest include LIDAR sensing of the atmosphere. Presently, he is working as an associate professor in ECE Department in Geethanjali College of Engineering and Technology, Hyderabad.